Mechanical Systems and Signal Processing 138 (2020) 106542

Contents lists available at ScienceDirect

Mechanical Systems and Signal Processing

journal homepage: www.elsevier.com/locate/ymssp

Nonlinear modeling of composite wing with application to UAV flight dynamic analysis

Yong-liang Guan [a], Wei Xu [b], Ming-yue Zhang [c,*]

[a] ChangGuang Satellite Technology Co., Ltd, Changchun 130052 China
[b] Changchun Institute of Optics, Fine Mechanics and Physics, Chinese Academy of Sciences, Changchun 130033, China
[c] Qingdao University of Science and Technology, Qingdao 266426, China

ARTICLE INFO

Article history:
Received 16 May 2019
Received in revised form 19 November 2019
Accepted 23 November 2019
Available online 5 December 2019

Keywords:
Composite wing
Geometric nonlinearity
Model identification
Flight simulation
Flight test

ABSTRACT

Wings have obvious nonlinear vibrations such as buffeting and flutter during the flight of the aircraft, the nonlinear vibrations are harmful to the safety of wing structures and stability of aircraft flight. Thereby, studying nonlinear dynamic characteristics of wings is extremely important, which makes the accurate nonlinear dynamic model urgently needed. For composite wings, traditional modeling theory cannot accurately predict the variability caused by manufacturing process, machining behavior and operating condition. Therefore, this paper used a numerical-experimental method to establish the dynamic model of a composite wing, considering geometric nonlinearity. In the method, the nonlinear dynamic model of the composite wing was predicted by an experimental modal analysis with a frequency response function, and a nonlinear static test with the nonlinear least squares method. Then, the nonlinear modeling was applied to a UAV flight dynamic simulation and a flight test was also conducted. The results of the simulation are in good agreement with those of the test, which shows that the nonlinear modeling is perfectly suited for the nonlinear dynamic analysis of the composite wing.

1. Introduction

Aerodynamic forces are unsteady during aircraft flight processes, which would cause nonlinear vibrations such as buffeting and flutter, due to the nonlinearity of wings, especially geometric nonlinearity [1–4]. Buffeting and flutter are both harmful to the safety of wing structures and stability of aircraft flight, so considering structural nonlinear dynamic characteristics in the design of wings is an extremely important, which makes accuracy nonlinear dynamic analysis of wings become an urgent need [5].

Composite materials frequently appear in the aviation field, increasing numbers of wings are being made of composite materials. The dynamic analysis of composite structures has recently attracted more attention, and many excellent theories are available on the finite element method for composite structural analysis [6]. The classical lamination theory is based on the Kirchhoff plate theory, which assumes that a plane section initially normal to the midsurface before deformation remains plane and normal to that surface after deformation. The first-order shear deformation theory can be considered as improvements over the classical Kirchhoff thin plate theory, which is achieved by including a total transverse shear deformation in the kinematic assumptions. Various higher-order shear deformation theories have overcome limitations both in the classical and first-order shear deformation theories, which includes both bending and shear effects. The layer-wise lamination theory

* Corresponding author.
E-mail address: zhangmingyue_paper@163.com (M.-y. Zhang).

https://doi.org/10.1016/j.ymssp.2019.106542
0888-3270/

assumes a displacement representation formula in each layer which can predict interlaminar stresses accurately, and the theory based on the 3D continuum can predict a composite laminate's interlaminar stress [7].

The theories have made significant progress. However, to obtain accurate dynamic response, we not only need for the appropriate theoretical model, but also for high-precision composite material performance parameters. But due to its complex manufacturing process and special material performance, there is an obvious variability in the mechanical properties of composite structures [8–14]. To ensure high reliability of structures, the actual behaviors of composite parts in service must be accurately predicted and carefully monitored. Therefore, it is essential to capture and model the variability inherent in these material properties [15].

The properties of composites can be obtained accurately via experimental tests [16], so the mixed numerical-experimental technique is applied to extract the physical information of composites. This usually involves minimizing an error function between the experimental and numerical outputs [8]. Constructing of predictive computational models for analysis and design of many complex engineering systems requires not only a fine representation of relevant physics and their interactions but also a quantitative assessment of underlying variability and their impact on design performance objectives [17]. Hence, a thorough characterization of the mechanical properties of these structures is needed to establish reliable designs. Mota [18] identified elastic properties of laminated composites by using experimental eigenfrequencies. The stiffness parameters were identified from the measured natural frequencies of the laminated composites plate by direct minimization of the identification function. A similar method was used by Frederiksen [19] and Araújo [20]. Frederiksen improved the model used for identification. Araújo used a mixed numerical-experimental technique to identify the damping properties of plyometric composites. Cunha [21] identified several properties of a composite plate from a single test. Diveyev [22] predicted the elastic and damping properties of composite laminated plates on the basis of static three-point bending tests, measured eigenfrequencies, and refined calculation schemes. Rikards [23] identified the elastic properties of cross-ply laminates from the measure eigenfrequencies of composite plates.

The mixed numerical-experimental technique makes the finite element method suitable for dynamic analysis of laminated composites. However, the tests for measuring the eigenfrequencies of composite plates are almost all linear as in the works mentioned above, and do not consider the structural nonlinearities of the laminated composites. There is obvious geometric nonlinearity in the work process of wings, so the nonlinear system identification is needed in the nonlinear dynamic analysis of composite wings. Our study is aimed at expanding a numerical-experimental method based on linear and nonlinear tests for nonlinear modeling and dynamic analysis of a composite wing.

2. Numerical-experimental method

The equation of motion of an n-degree-of-freedom nonlinear system can be written in the form:

$$M\ddot{x}(t) + C\dot{x}(t) + Kx(t) + K_u x(t) = F(t) \tag{1}$$

where $\boldsymbol{M}$ and $\boldsymbol{K}$ are the real symmetric mass and stiffness matrices, respectively. $\boldsymbol{C}$ is the damping of the system. $\boldsymbol{x}(t)$ and $\boldsymbol{F}(t)$ are the displacements and external load vectors, respectively. $\boldsymbol{K_u}$ is the stiffness component dependent on displacements. For the relevant problems, the nonlinear stiffness force vector $\boldsymbol{K_u x}(t)$ represents a deviation from the linear stiffness force vector $\boldsymbol{Kx}(t)$ and is more than adequately represented by second- and third-order terms in $\boldsymbol{x}(t)$. When displacements are small, the second- and third-order terms become negligible and the total stiffness-related force vector is reduced to the regular linear term $\boldsymbol{Kx}(t)$.

Any solution to Eq. (1) requires the knowledge of the system matrices. In the linear identification works mentioned above, $\boldsymbol{M}$, $\boldsymbol{K}$, and $\boldsymbol{C}$ are generally available. The nonlinear parameters, which are related to $\boldsymbol{K_u}$, are typically not available within a linear identification work. Therefore, a mean of numerically evaluating $\boldsymbol{M}$, $\boldsymbol{K}$, $\boldsymbol{C}$ and $\boldsymbol{K_u}$ was developed.

A set of coupled modal equations with reduced degrees-of-freedom is first obtained by applying the modal coordinate transformation:

$$x(t) = \Phi \boldsymbol{q}(t) \tag{2}$$

where $\boldsymbol{\Phi}$ is the eigenvector matrices of the model defined in Eq. (1) without $\boldsymbol{K_u}$, and $\boldsymbol{q}(t)$ is the vector of the displacement modal coordinates for each time instant t.

Then, Eq. (1) can be expressed as:

$$\tilde{M}\,\ddot{q}(t) + \tilde{C}\,\dot{q}(t) + \tilde{\mathrm{K}}\,q(t) + \tilde{\mathrm{K}}_u q(t) = \tilde{F}\,(t) \tag{3}$$

where

$$\begin{aligned}
&\tilde{M} = \Phi^T M \Phi = \mathrm{I} \\
&\tilde{C} = \Phi^T C \Phi = 2\xi\boldsymbol{\omega} \\
&\tilde{\mathrm{K}} = \Phi^T K \Phi = \boldsymbol{\omega^2} \\
&\tilde{\mathrm{K}}_u = \Phi^T K_u \Phi = \chi(q) \\
&\tilde{F}\,(t) = \Phi^T F(t)
\end{aligned} \tag{4}$$

and, $\boldsymbol{\omega}$ is the eigenvalue matrices of the model defined in Eq. (1) and ξ is the damping ratio of the model.

Then, Eq. (3) can be written as:

$$\ddot{\boldsymbol{q}}(t) + 2\xi\boldsymbol{\omega}\dot{\boldsymbol{q}}(t) + \boldsymbol{\omega}^{\boldsymbol{2}}\boldsymbol{q}(t) + \boldsymbol{\chi}(\boldsymbol{q})\boldsymbol{q}(t) = \Phi^{\mathrm{T}}F(t) \tag{5}$$

When the modal coordinate transformation is introduced and the nonlinearity is not obvious, Eq. (5) can be written as a system with only linear part, which is available within a linear identification work:

$$\ddot{\boldsymbol{q}}(t) + 2\xi\boldsymbol{\omega}\dot{\boldsymbol{q}}(t) + \boldsymbol{\omega}^{\boldsymbol{2}}\boldsymbol{q}(t) = \Phi^{\mathrm{T}}F_m(t) \tag{7}$$

where $\boldsymbol{F_m}$(t) is linear dynamic load.

When the system is static, Eq. (3) can be written as:

$$\boldsymbol{\chi}(\boldsymbol{q})\boldsymbol{q}(t) = \Phi^{\mathrm{T}}F_s(t) - \boldsymbol{\omega}^{\boldsymbol{2}}\boldsymbol{q}(t) \tag{8}$$

where $\boldsymbol{F_s}(t)$ is nonlinear static load.

In the numerical-experimental method of this paper, the linear part of the nonlinear system shown in Eq. (7) was identified by experimental eigenvalue matrices, eigenvector matrices, and others from an experimental modal analysis, in which the nonlinearity is not obvious. And the nonlinear part shown in Eq. (8) was identified by a nonlinear static test. The flowchart of the numerical-experimental method of this paper is shown in Fig. 1.

2.1. Linear parameters identification

The linear parameters were identified by the experimental modal analysis. The experimental modal analysis is a method to describe a structure in terms of its natural characteristics which are the frequencies, damping and mode shapes with the signal-analysis techniques.

The frequency spectrum is the description of how vibration levels vary with frequencies which can then be checked against a specification. The frequency response function measurement removes forces spectrum from the data and describes the inherent structural response between defined points on the structure.

In the frequency domain, the transfer matrix of output and input of an n-degree-of-freedom system is generally given by [24]:

$$H(\omega) = \left(K + i\omega C - \omega^2 M\right)^{-1} \tag{9}$$

The matrix $\boldsymbol{H}(\omega)$ is usually called the frequency response matrix. $\boldsymbol{\omega}$, ξ and $\boldsymbol{\Phi}$ in Eq. (7), which are the eigenvalue, damping and eigenvector matrices of the model, could be obtained from $\boldsymbol{H}(\omega)$.

2.2. Nonlinear parameters identification

The nonlinear parameters were identified by the nonlinear static test. Muravyov [25] and Mignolet [26] et al. wrote the dynamic equations in the modal coordinates and determined the nonlinear stiffness coefficients by combining the linear modes. For dynamic analysis, the process of obtaining the nonlinear stiffness coefficients replaces the procedure of solving the change of modal shapes and frequencies caused by deflection, and the verification results in their works show that the method has enough accuracy for the dynamic analysis.

The nonlinear force vector of Eq. (8) may be expressed in the form [25–28]:

$$\boldsymbol{\chi}(\boldsymbol{q})\boldsymbol{q}(t) = \sum_{j=1}^{l}\sum_{k=j}^{l} a_{jk}^{r} q_j q_k + \sum_{j=1}^{l}\sum_{k=j}^{l}\sum_{m=k}^{l} b_{jkm}^{r} q_j q_k q_m \tag{10}$$

where a^r and b^r are the rth line identification parameters of the nonlinear force vector. $r = 1, 2, \ldots l$. $l \leq n$, which is the number of modes used in parameters identification.

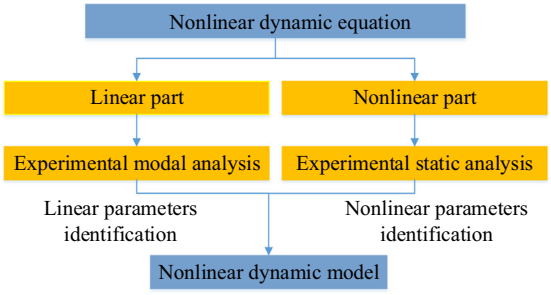

Fig. 1. Flowchart of numerical-experimental method.

The nonlinear parameters a^r and b^r in Eq. (10) were identified by the nonlinear static test based on the nonlinear least squares method. The nonlinear least squares method is one of the most common problems encountered in practical data analysis, and involves the fitting of a theoretical model to experimental data. Frequently, the model takes the form of a dependent variable expressed as a function of several independent variables. Often the model will contain one or more estimated parameter. This estimation occurs on the basis of fitting the model to observations using the least-squares method.

Then, the nonlinear dynamic model is built after the linear parameters $\boldsymbol{\omega}$, $\boldsymbol{\Phi}$ and $\boldsymbol{\xi}$, and the nonlinear parameters a^r and b^r are identified.

3. Nonlinear modeling of composite wing

3.1. Composite wing

The composite wing as shown in Fig. 2 is considered as follows. The airfoil profile of the composite wing is NACA 4415. The length of the wing is 1500 mm, the root chord is 600 mm, and the tip chord is 270 mm. Although the aspect ratio of the wing is not particularly high, the geometric nonlinearity is still very noticeable when the UAV is flying at high speed.

The layout of the wing structure is shown in Fig. 3.

Three composite materials, which are the woven fiberglass cloth, the 3 k woven carbon fiber cloth and the foam core are used in the manufacture of the wing. The structural components of the composite wing, described in Table 1, are composited by different materials, respectively.

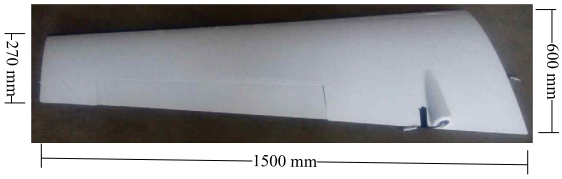

Fig. 2. Composite wing.

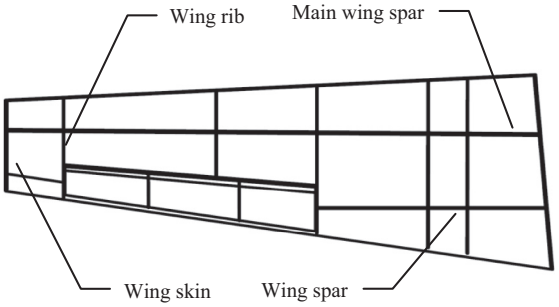

Fig. 3. Layout of wing structure.

Table 1
Material composition versus wing component.

Component	Material composition
Wing skin	Woven fiberglass cloth Foam core
Main wing spar	Woven fiberglass cloth 3 k Woven carbon fiber cloth Foam core
Wing spar	Woven fiberglass cloth Foam core
Wing rib	Woven fiberglass cloth Foam core

3.2. Linear parameters identification of composite wing

The linear parameters of the composite wing were identified by experimental modal analysis. In general, the database is obtained from direct measurements. The frequency response functions are then measured, and have been used to properly arrange the experimental setup used for the identification of the linear parameters.

The composite wing was tested in fixed constraint at the wing root, which is closed to the working condition, as shown in Fig. 4.

The sensors were located on the upper surface of the composite wing, as shown in Fig. 5.

The frequency response functions (FRFs) were computed by a data acquisition and analysis system LMS SCADAS III, and the experimental natural frequencies and modal shapes were obtained by modal analyses using LMS Test. Lab Structure Analysis. Fig. 6 shows the FRFs result of the point 4.

Table 2 gives the first twenty frequencies of each mode.

The first six modal shapes are shown in Fig. 7.

Then, $\boldsymbol{\omega}$, $\boldsymbol{\xi}$ and $\boldsymbol{\Phi}$ in Eq. (7), which are the eigenvalue, damping and eigenvector matrices of the model were obtained from the experiment results.

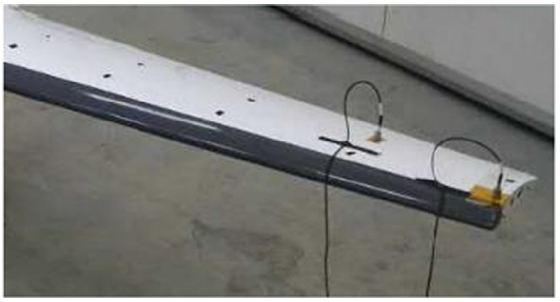

Fig. 4. Setup of experimental modal analysis.

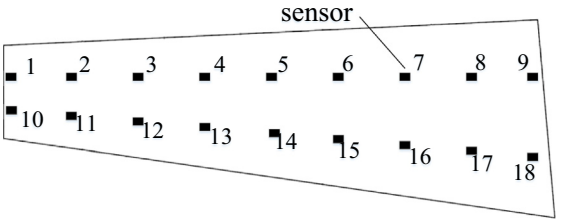

Fig. 5. Locations of sensors.

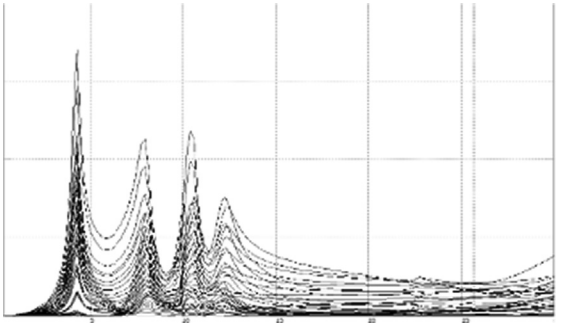

Fig. 6. FRFs result of point 4.

Table 2
Frequency versus mode number.

Mode	Frequency/Hz	Mode	Frequency/Hz
1	30.03	11	412.22
2	93.24	12	425.02
3	104.23	13	449.29
4	121.06	14	459.12
5	194.89	15	466.79
6	305.18	16	488.89
7	292.19	17	519.85
8	313.57	18	536.43
9	346.39	19	554.97
10	378.51	20	561.28

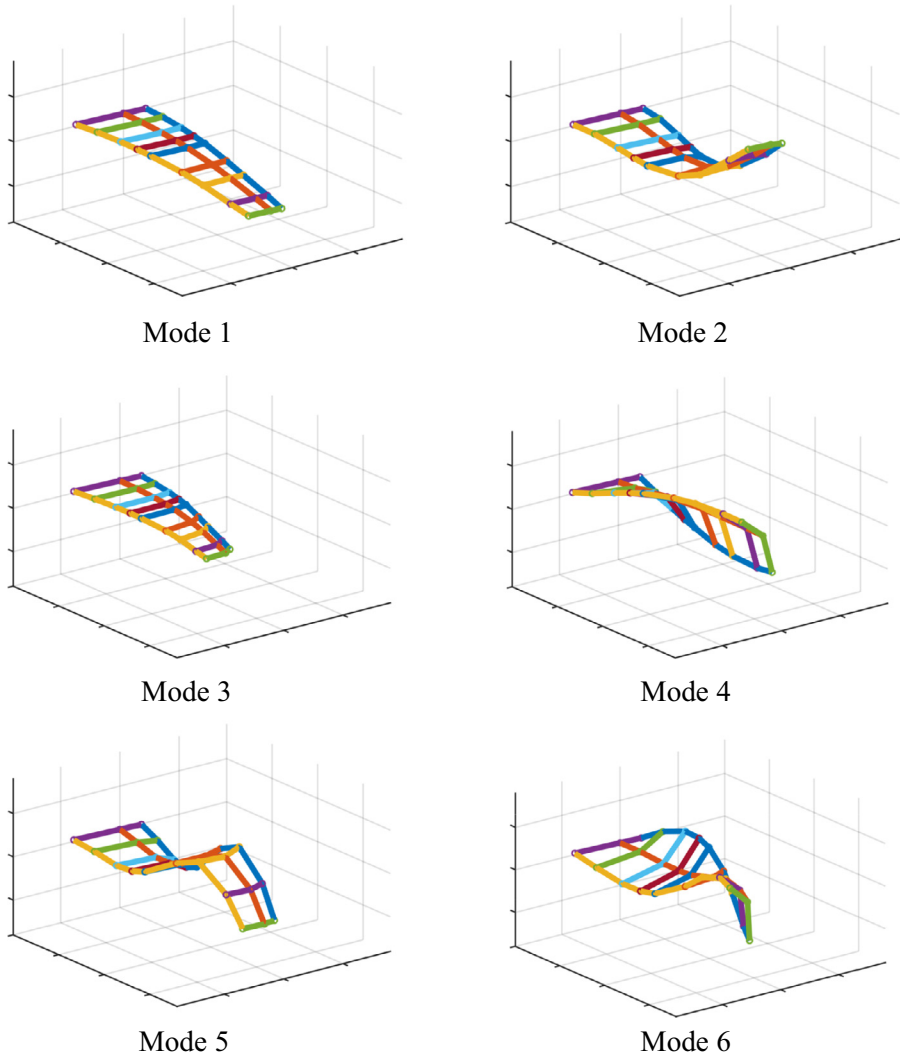

Fig. 7. Modal shapes of composite wing.

3.3. Nonlinear parameters identification of composite wing

The nonlinear parameters of the composite wing were identified by a nonlinear static test. The test was performed in fixed constraint at the wing root, and loads were applied on the upper surface of the wing, as shown in Fig. 8.

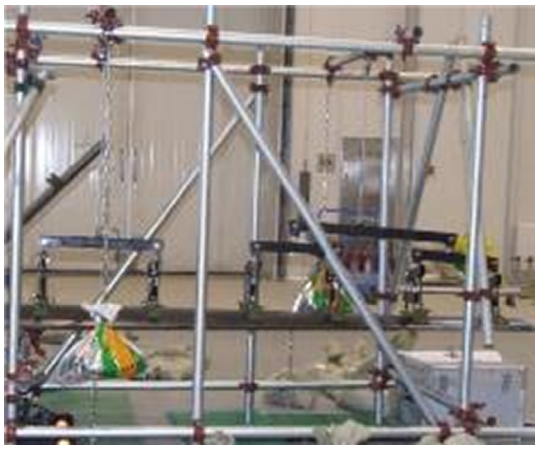

Fig. 8. Setup of nonlinear static test.

The loads varied from 54 N to 1080 N with the increment of 54 N. The wing was divided into six areas as shown in Fig. 9. Loads calculated by fluid analysis were applied to these areas.

The displacement of the wingtip changed as the load changed. The changes were measured by a height caliper, and the displacements under different loads are shown in Table 3.

The nonlinear parameters of the composite wing were identified by Eqs. (8) and (10) with the nonlinear least squares method based on the results of the nonlinear static test.

$$\sum_{j=1}^{l}\sum_{k=j}^{l} a_{jk}^{r} q_j q_k + \sum_{j=1}^{l}\sum_{k=j}^{l}\sum_{m=k}^{l} b_{jkm}^{r} q_j q_k q_m = \Phi^{\mathrm{T}} F_s(t) - \boldsymbol{\omega^2} q(t) \tag{11}$$

The displacements of the wingtip under different loads were recalculated after the nonlinear parameters were identified. The results of the identification were compared with the displacement-loading curve of the nonlinear static test, as shown in Fig. 10.

Fig. 10 shows that the wing has obvious geometric nonlinearity, and the results of the identification are not obviously different than the results of the nonlinear static structural test.

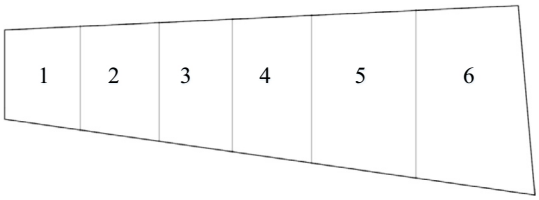

Fig. 9. Loads application areas.

Table 3
Results of nonlinear static test.

Load/N	Displacement/mm	Load/N	Displacement/mm
54	4.50	594	46.53
108	8.98	648	50.15
162	13.44	702	53.60
216	17.85	756	56.88
270	22.22	810	59.96
324	26.52	864	62.93
378	30.73	918	65.62
432	34.86	972	68.08
486	38.88	1026	70.29
540	42.77	1080	72.25

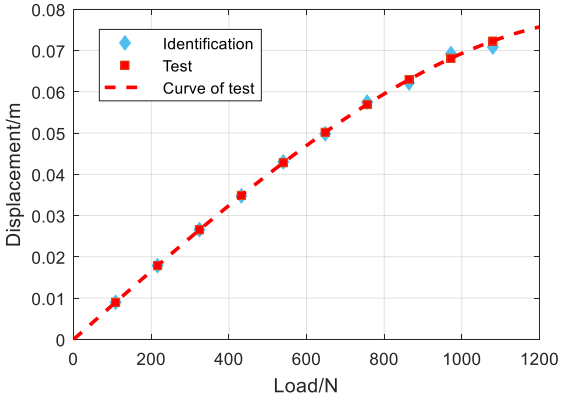

Fig. 10. Result comparison of identification and test.

4. Flight dynamic analysis

The nonlinear modal of the composite wing was used in a flight dynamic analysis of a UAV. The maximum weight of the aircraft is 160 kg, and the maximum speed is 370 km/h. In the process of flight, the variation of the flight state leads to the unsteady aerodynamic forces, the unsteady aerodynamic forces cause the nonlinear vibration of the wing, the nonlinear vibration brings the variation in the flight state, and the cycle repeats. The wing has obvious nonlinear vibrations in the process of flight. Thereby, the nonlinear modeling method of the composite wing was applied to a flight dynamic simulation. Then, to check the accuracy and practicability of the method, the simulation results were compared with the results of a flight test.

4.1. Method for flight dynamic simulation

4.1.1. Solution of nonlinear equations

To solve the nonlinear dynamic model show in Eq. (5), it was projected in the modal space:

$$\dot{\boldsymbol{z}}(t) = \boldsymbol{D}\boldsymbol{z}(t) + \boldsymbol{D}_{\boldsymbol{x}}\boldsymbol{z}(t) + \boldsymbol{V}F(t) \tag{12}$$

where

$$\boldsymbol{z}(t) = \begin{Bmatrix} \boldsymbol{q}(t) \\ \dot{\boldsymbol{q}}(t) \end{Bmatrix} \quad \boldsymbol{V} = \begin{Bmatrix} 0 \\ \Phi^{\mathrm{T}} \end{Bmatrix} \boldsymbol{D} = \begin{bmatrix} 0 & I \\ -\boldsymbol{\omega}^2 & -2\xi\boldsymbol{\omega} \end{bmatrix} \quad \boldsymbol{D}_{\boldsymbol{x}} = \begin{bmatrix} 0 & 0 \\ -\boldsymbol{\chi}(q) & 0 \end{bmatrix} \tag{13}$$

Giuseppe Muscolino [29] put forward a new approach to convert the modal space to a iterative equation in discrete time. Divide the time axis in small intervals of equal length Δt and let $t_0, t_1, \ldots, t_k, t_{k+1}, \ldots$ be the division time. Then, the numerical solution of Eq. (12) can be written as follows:

$$\boldsymbol{z}_{k+1} = \Gamma_1(\Delta t)\boldsymbol{D}_{\boldsymbol{x}}(\boldsymbol{z}_{k+1})\boldsymbol{z}_{k+1} + (\Theta_0(\Delta t) + \Gamma_0(\Delta t)\boldsymbol{D}_{\boldsymbol{x}}(\boldsymbol{z}_k))\boldsymbol{z}_k + \Gamma_0(\Delta t)\boldsymbol{V}\boldsymbol{F}_k + \Gamma_1(\Delta t)\boldsymbol{V}\boldsymbol{F}_{k+1} \tag{14}$$

where

$$\boldsymbol{z}_k = \boldsymbol{z}(t_k) \qquad \boldsymbol{F}_k = \boldsymbol{F}(t_k) \tag{15}$$

and,

$$\begin{aligned} \boldsymbol{L}(\Delta t) &= [\Theta_0(\Delta t) - \boldsymbol{I}]\boldsymbol{D}^{-1} \\ \boldsymbol{\Gamma}_0(\Delta t) &= \left[\Theta_0(\Delta t) - \tfrac{1}{\Delta t}\boldsymbol{L}(\Delta t)\right]\boldsymbol{D}^{-1} \\ \boldsymbol{\Gamma}_1(\Delta t) &= \left[\tfrac{1}{\Delta t}\boldsymbol{L}(\Delta t) - \boldsymbol{I}\right]\boldsymbol{D}^{-1} \end{aligned} \tag{16}$$

$\boldsymbol{\Theta}_0(t)$ is the so-called transition or fundamental matrix which is given as [29]:

$$\Theta_0(t) = \begin{bmatrix} -\boldsymbol{g}(t)\omega^2 & \boldsymbol{h}(t) \\ -\boldsymbol{h}(t)\boldsymbol{\omega}^2 & \dot{\boldsymbol{h}}(t) \end{bmatrix} \tag{17}$$

where $\boldsymbol{g}(t)$, $\boldsymbol{h}(t)$, $\dot{\boldsymbol{g}}(t)$ and $\dot{\boldsymbol{h}}$ (t) are diagonal matrices whose jth elements are given, respectively, as:

$$
\begin{aligned}
g_j(t) &= -\frac{1}{\omega_j^2}e^{-\xi_j\omega_j t}\cos(\omega_{Dj}t) - \frac{1}{\omega_j^2}e^{-\xi_j\omega_j t}\frac{\xi_j\omega_j}{\omega_{Dj}}\sin(\omega_{Dj}t)\\
h_j(t) &= \dot{g}_j(t) = \frac{1}{\omega_{Dj}}e^{-\xi_j\omega_j t}\sin(\omega_{Dj}t)\\
\dot{h}_j(t) &= e^{-\xi_j\omega_j t}\cos(\omega_{Dj}t) - e^{-\xi_j\omega_j t}\frac{\xi_j\omega_j}{\omega_{Dj}}\sin(\omega_{Dj}t)
\end{aligned}
\tag{18}
$$

and,

$$
\omega_{Dj} = \omega_j\sqrt{1-\xi_j^2} \tag{19}
$$

is the jth damped natural frequency.

Then, Eq. (14) can be written as follows:

$$
(I - \boldsymbol{\Gamma}_1(\Delta t)\boldsymbol{D}_{\boldsymbol{x}}(\boldsymbol{z}_{k+1}))\boldsymbol{z}_{k+1} = (\boldsymbol{\Theta}_0(\Delta t) + \boldsymbol{\Gamma}_0(\Delta t)\boldsymbol{D}_x(\boldsymbol{z}_k))\boldsymbol{z}_k + (\boldsymbol{\Gamma}_0(\Delta t)\boldsymbol{V}\boldsymbol{F}_k + \boldsymbol{\Gamma}_1(\Delta t)\boldsymbol{V}\boldsymbol{F}_{k+1}) \tag{20}
$$

The solution process of Eq. (20) was nonlinear, so an iterative method was needed. The iterative method used here was the Newton Raphson method. The convergence criterion of the iterative process was based on the minimum 2-norm. In the solution process of Eq. (20), while

$$
\| \boldsymbol{z}_{k+1} - \boldsymbol{z}_k \|_2 \leqslant CRIT \tag{21}
$$

the results are convergent.

4.1.2. Aerodynamic forces

The aerodynamic forces of the wing are unsteady during the flight process, and the unsteady aerodynamic parameters of the composite wing are derived from a previous experiment. The lift coefficients of the composite wing under different dynamic pressure are shown in Fig. 11. The drag coefficients are shown in Fig. 12, and the pitch moment coefficients are shown in Fig. 13. 0, 25, …, 200 are dynamic pressures measured in psf.

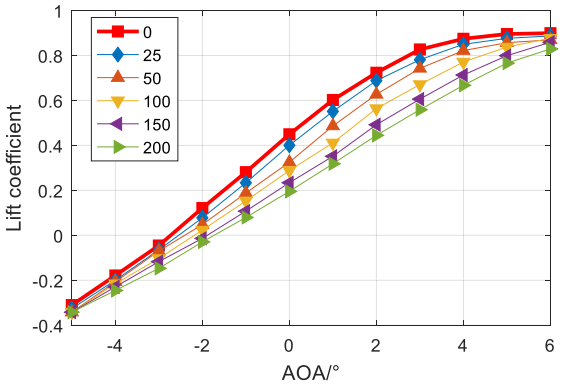

Fig. 11. Lift coefficients of composite wing.

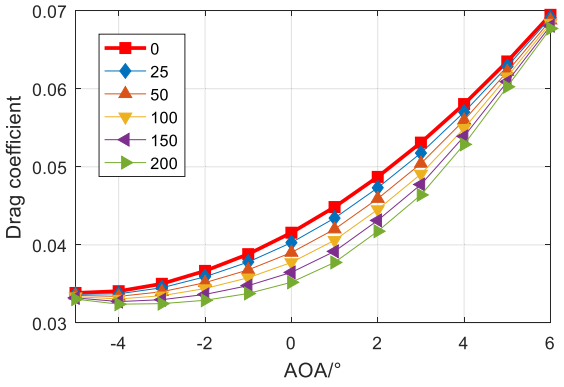

Fig. 12. Drag coefficients of composite wing.

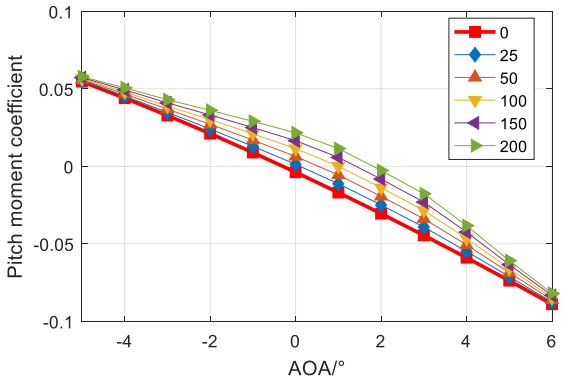

Fig. 13. Pitch moment coefficients of composite wing.

The aerodynamic parameters were tabulated in multi-dimensional look-up tables, and the aerodynamic forces and moments of different flight states were then computed from the database with a multi-linear interpolation.

4.1.3. Equations of motion

The aircraft equations of motion are derived from the Newton's law of translational and rotational motions. The translational equations can be written as

$$m\frac{d\boldsymbol{V}}{dt} = \sum \boldsymbol{F} \tag{22}$$

where $\boldsymbol{V}$ is the velocity vector of the aircraft, m is the mass of the aircraft, $\boldsymbol{F}$ is the external load applied on the aircraft.

The rotational equations of motion are given as:

$$\frac{d\boldsymbol{H}}{dt} = \sum \boldsymbol{M} \tag{23}$$

where $\boldsymbol{H}$ is the angular momentum of the aircraft, $\boldsymbol{M}$ is the external torque applied on the aircraft. The equations of motion in this paper were solved by the Runge–Kutta fourth-order method.

4.1.4. Interaction method

The flight dynamic simulation involves a significant mutual interaction of aerodynamic forces, wing deformations and flight motion, and the interaction method is described in Fig. 14. The processes shown in Fig. 14 are:

1. Get flight state at time t from equations of motion, and pass it to the fluid-structural coupling;
2. Calculate aerodynamic forces and bring them into nonlinear structural modeling;
3. Solve nonlinear structural equations until it converges;
4. Bring wing deflections to fluid;
5. Interpolate aerodynamic parameters and calculate aerodynamic forces;
6. After fluid-structural coupling converges, bring aerodynamic forces to equations of motion as the loads at time $t + \Delta t$.

4.2. Flight dynamic simulation

The mission profile of the flight dynamic simulation is illustrated in Fig. 15.

The processes shown in Fig. 15 are:

1. Take off by catapult at pitch angle of 7°;
2. Climb at pitch angle of 11° to 1000 m;
3. Maintain altitude of 1000 m at velocity of 100 m/s;
4. Descend at pitch angle of −6° to 500 m;
5. Maintain altitude of 500 m at velocity of 150 m/s;
6. Climb at pitch angle of 11° to 750 m;
7. Maintain altitude of 750 m at velocity of 100 m/s;
8. Descend at pitch angle of −6° and prepare to land;
9. Landing.

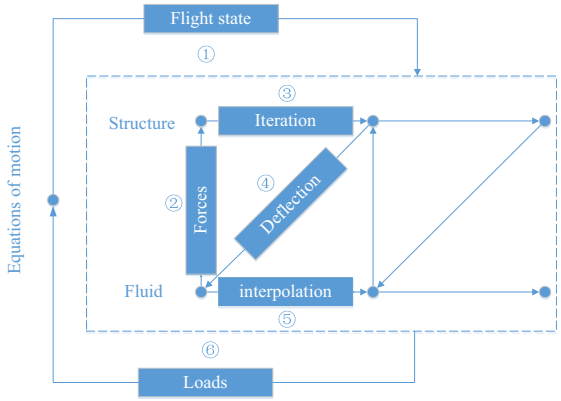

Fig. 14. Interaction process.

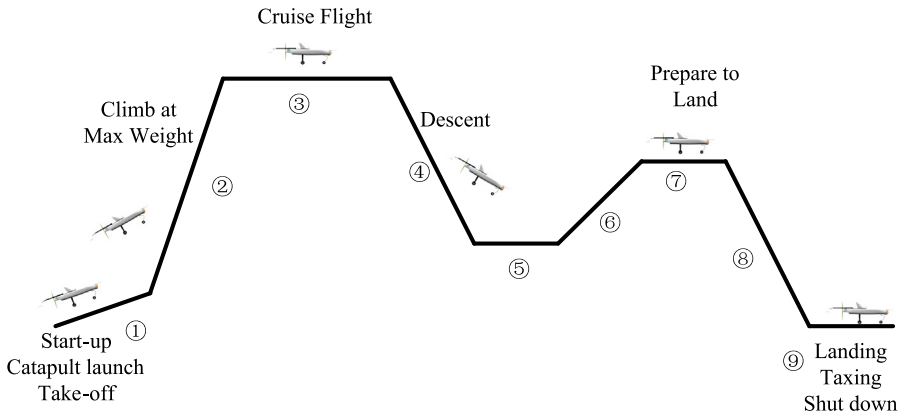

Fig. 15. Mission profile of flight dynamic simulation.

The flight state results of the flight dynamic simulation are shown in Figs. 16–18. Fig. 16 shows the altitude variation of the aircraft in the flight dynamic simulation. Figs. 17 and 18 show the curves of pitch angle and attack angle of the aircraft. Fig. 16 shows that the flight curve of the aircraft is consistent with the mission requirement, which indicates that the results of this analysis have a high degree of credibility. It can be seen from Figs. 17 and 18 that the pitch angle and attack angle of the aircraft change very sharply over time, it is because that the analysis considered the effect of wing deformation on aerodynamic loads. The curve will become gentle if not consider this effect, but results will be far from reality.

The dynamic response results of the composite wing are shown in Figs. 19–22. Fig. 19 shows the lift variation of the composite wing in the flight dynamic simulation. Fig. 20 shows the drag variation and Fig. 21 shows the pitch moment variation. Fig. 22 shows the response of the wingtip in the vertical direction.

The interactions among aerodynamics, stiffness, and inertial forces leaded to oscillations in the aerodynamic load curves as shown in Figs. 19–21, the oscillations were then attenuated by the structural damping of the wing. If the structural damping could not attenuate these vibrations, buffeting would occur, even flutter.

Comparing Fig. 19 with Fig. 10, it can be seen that the maximum lift of the wing has reached 1400 N, far exceeding 800 N, which is the starting load for the nonlinear deformation of the wing. In this flight analysis, there has been a significant aeroelastic phenomenon, which is also shown in Fig. 22. If only the linear model is used for the analysis, without considering the effect of the wing nonlinearity, it is not possible to accurately evaluate aerodynamic loads and wing deformation, nor to properly observe the aeroelastic response of the wing. This would result in wing mechanical properties not accurately verified thus making impossible to judge when and how the buffeting and flutter occur.

4.3. Flight test results

A flight test was conducted in Chang Chun, Ji Lin Province of China, as shown in Fig. 23. The mission profile of the flight test is the same as that of the flight dynamic simulation as shown in Fig. 15.

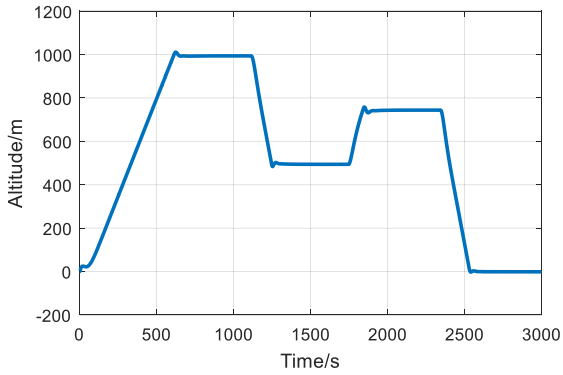

Fig. 16. Curve of altitude in flight simulation.

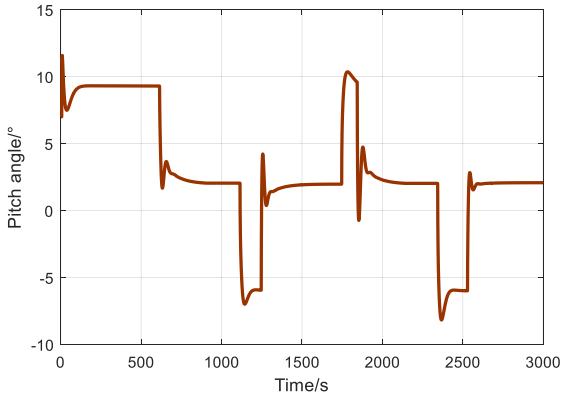

Fig. 17. Curve of pitch angle in flight simulation.

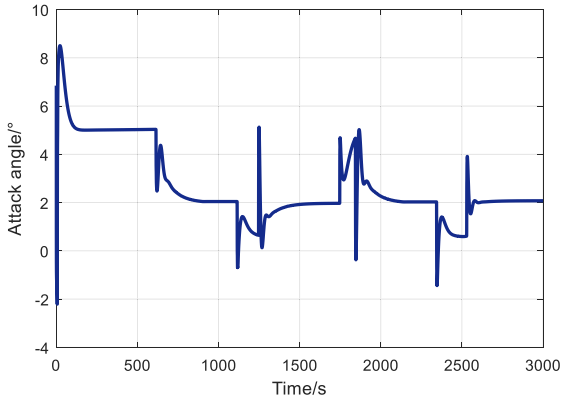

Fig. 18. Curve of attack angle in flight simulation.

The data of flight test was collected by the angle of attack sensor and the integrated navigation system. The results of flight were composed with those of the flight dynamic simulation, as shown in Figs. 24–26. Fig. 24 shows the altitude comparison result of the flight dynamic and flight test. Fig. 25 and Fig. 26 show the comparison results of the pitch angle and attack angle.

Figs. 24–26 show that the results of the flight dynamic simulation are in good agreement with those of the flight test, which indicates that the method has the characteristic of high emulation accuracy, the nonlinear modeling of composite wing is suitable to the flight dynamic of aircraft and could well reflect the dynamic performance of the composite wing.

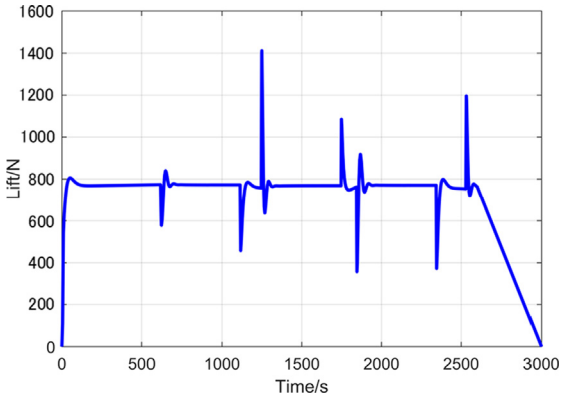

Fig. 19. Curve of lift in flight simulation.

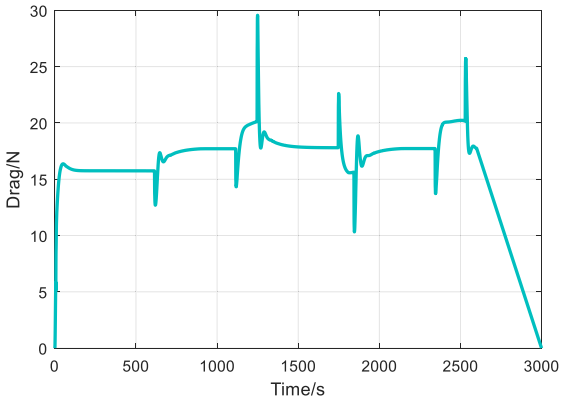

Fig. 20. Curve of drag in flight simulation.

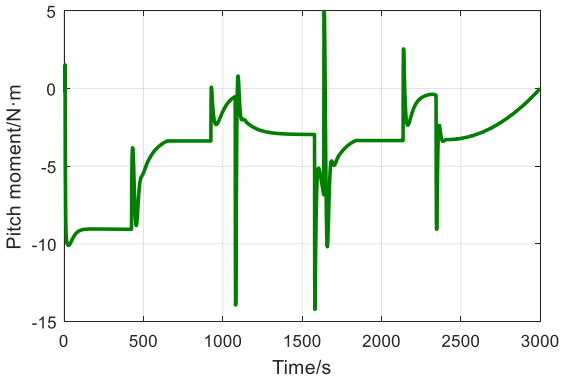

Fig. 21. Curve of pitch moment in flight simulation.

5. Conclusion

Since the variability in mechanical properties must be considered in the nonlinear dynamic analysis of composite structures, the nonlinear modeling of a composite wing is built by a numerical-experimental method, which could predict the dynamic performance of the composite wing accurately. In the method, the linear parameters are predicted by an experimental modal analysis with a frequency response function, and a nonlinear static test is employed to identify the nonlinear parameters with the nonlinear least squares method.

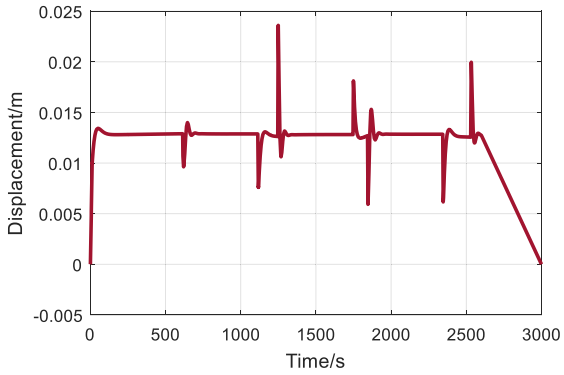

Fig. 22. Response of wingtip in vertical direction.

Fig. 23. Flying aircraft in flight test.

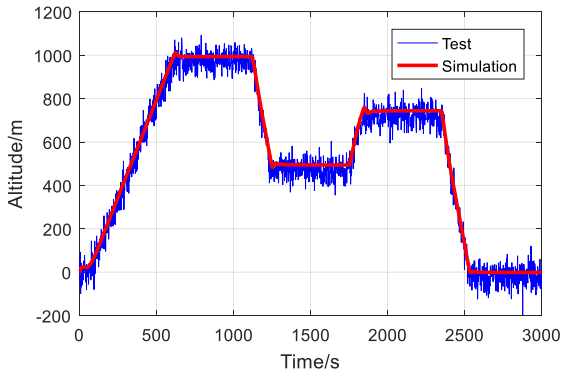

Fig. 24. Comparison result of altitude.

To check the accuracy and practicability of the nonlinear modeling, it was applied to a flight dynamic analysis of the aircraft based on the interaction of geometric nonlinear modeling, aerodynamic forces and equations of motion. Then, the results of the flight dynamic simulation were compared with those of a flight test. The comparison results show that the results of the flight dynamic simulation are in good agreement with those of the flight test, which indicates that the nonlinear modeling is perfectly suitable for the dynamic analysis of the composite wing.

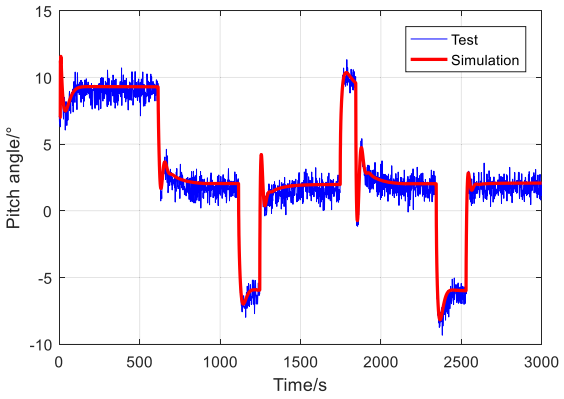

Fig. 25. Comparison result of pitch angle.

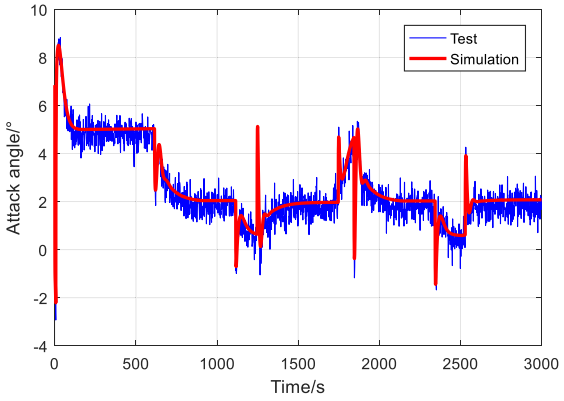

Fig. 26. Comparison result of attack angle.

The nonlinear modeling method proposed in this paper identifies the dynamic characteristics of the composite wing based on the tests, and solves the problem that the existing theoretical modeling method does not have enough precision. The method is not only applicable to the composite wing used in this paper, but also to any composite structure, and even most mechanical structures can be nonlinearly modeled by this method.

The flight analysis method of UAV used in this paper can accurately obtain the state data of aircrafts such as the pitch angle and the angle of attack, which provides a good foundation for the flight control of aircrafts. Through flight analysis, the aerodynamic loads and deformation of wings can also be accurately determined. Based on this, it is easy to judge the occurrence conditions of buffeting and flutter, which is of great significance not only to the structural safety of wings, but also to the flight safety of the aircrafts.

CRediT authorship contribution statement

Yong-liang Guan: Methodology, Software, Validation, Formal analysis, Investigation, Writing - original draft, Writing - review & editing, Visualization, Supervision, Project administration. **Wei Xu:** Resources, Funding acquisition. **Ming-yue Zhang:** Conceptualization, Data curation.

Acknowledgements

The project was supported by the Knowledge Innovation Program of the Chinese Academy of Sciences (Grant No. YYYJ-1122) and the Innovation Program of UAV funded by the ChangGuang Satellite Technology Co., Ltd. The authors also gratefully acknowledge the support from the Science Fund for Young Scholars of the National Natural Science Foundation of China (Grant No. 51305421).

Appendix A. Supplementary data

Supplementary data to this article can be found online at https://doi.org/10.1016/j.ymssp.2019.106542.

References

[1] M. Candon, R. Carrese, H. Ogawa, P. Marzocca, C. Mouser, O. Levinski, W.A. Silva, Characterization of a 3DOF aeroelastic system with freeplay and aerodynamic nonlinearities – Part I: higher-order spectra, Mech. Syst. Sig. Process. 118 (2018) 781–807.
[2] M. Candon, R. Carrese, H. Ogawa, P. Marzocca, C. Mouser, O. Levinski, Characterization of a 3DOF aeroelastic system with freeplay and aerodynamic nonlinearities – Part II: hilbert-huang transform, Mech. Syst. Sig. Process. 114 (2018) 628–643.
[3] J. Ertveldt, J. Lataire, R. Pintelon, S. Vanlanduit, Frequency-domain identification of time-varying systems for analysis and prediction of aeroelastic flutter, Mech. Syst. Sig. Process. 47 (2014) 225–242.
[4] P.C.O. Martins, T.A.M. Guimarães, D.D.A. Pereira, F.D. Marques, D.A. Rade, Numerical and experimental investigation of aeroviscoelastic systems, Mech. Syst. Sig. Process. 85 (2017) 680–697.
[5] G. Georgiou, A. Manan, J.E. Cooper, Modeling composite wing aeroelastic behavior with uncertain damage severity and material properties, Mech. Syst. Sig. Process. 32 (2012) 32–43.
[6] Y. Guan, Z. Xue, M. Li, H. Jia, A Numerical-Experimental Method for Drop Impact Analysis of Composite Landing Gear, Shock and Vibration, 2017, (2017-6-13), 2017 (2017) 1-11.
[7] Y.X. Zhang, C.H. Yang, Recent developments in finite element analysis for laminated composite plates, Compos. Struct. 88 (2009) 147–157.
[8] L. Mehrez, D. Moens, D. Vandepitte, Stochastic identification of composite material properties from limited experimental databases, part I: Experimental database construction, Mech. Syst. Sig. Process. 27 (2012) 471–483.
[9] S. Sriramula, M.K. Chryssanthopoulos, Quantification of uncertainty modelling in stochastic analysis of FRP composites, Compos Part A-Appl. Sci. Manuf. 40 (2009) 1673–1684.
[10] J. Cao, R. Akkerman, P. Boisse, J. Chen, H.S. Cheng, E.F.D. Graaf, J.L. Gorczyca, P. Harrison, G. Hivet, J. Launay, Characterization of mechanical behavior of woven fabrics: experimental methods and benchmark results, Compos. A Appl. Sci. Manuf. 39 (2008) 1037–1053.
[11] H. Li, R. Foschi, R. Vaziri, G. Fernlund, A. Poursartip, Probability-based modelling of composites manufacturing and its application to optimal process design, J. Compos. Mater. 36 (2002) 1967–1991.
[12] P. Rakesh, V. Sharma, I. Singh, D. Kumar, Delamination in fiber reinforced plastics: A finite element approach, Engineering 3 (2011) 549.
[13] P.K. Rakesh, V. Sharma, I. Singh, D. Kumar, Delamination in Fiber Reinforced Plastics: A Finite Element Approach, Engineering 03 (2011).
[14] S. Pantelakis, K.I. Tserpes, Adhesive bonding of composite aircraft structures: challenges and recent developments, Sci. China-Phys. Mech. Astron. 57 (2014) 2–11.
[15] W. Qi, S. Tian, Z. Qiu, A novel stochastic collocation method for uncertainty propagation in complex mechanical systems, Sci. China Phys. Mech. Astron. 58 (2015) 1–8.
[16] D. Jiang, Y. Li, Q. Fei, S. Wu, Prediction of uncertain elastic parameters of a braided composite, Compos. Struct. 126 (2015) 123–131.
[17] L. Mehrez, A. Doostan, D. Moens, D. Vandepitte, Stochastic identification of composite material properties from limited experimental databases Part II: Uncertainty modelling, Mech. Syst. Signal Process. 27 (2012) 484–498.
[18] C.M.M. Soares, M.M.D. Freitas, A.L. Araújo, P. Pedersen, Identification of material properties of composite plate specimens, Compos. Struct. 25 (1993) 277–285.
[19] P.S. Frederiksen, Experimental procedure and results for the identification of elastic constants of thick orthotropic plates, J. Compos. Mater. 31 (1997) 360–382.
[20] A.L. Araújo, C.M.M. Soares, M.J.M.D. Freitas, Characterization of material parameters of composite plate specimens using optimization and experimental vibrational data, Compos. B Eng. 27 (1996) 185–191.
[21] J. Cunha, S. Cogan, C. Berthod, Application of genetic algorithms for the identification of elastic constants of composite materials from dynamic tests, Int. J. Numer. Meth. Eng. 45 (2015) 891–900.
[22] B. Diveyev, I. Butiter, N. Shcherbina, Identifying the elastic moduli of composite plates by using high-order theories, Mech. Compos. Mater. 44 (2008) 25–36.
[23] R. Rikards, A. Chate, G. Gailis, Identification of elastic properties of laminates based on experiment design, Int. J. Solids Struct. 38 (2001) 5097–5115.
[24] D.J. Ewins, Modal Testing: Theory and Practice, Research Studies Press Letchworth, 1984.
[25] A.A. Muravyov, S.A. Rizzi, Determination of nonlinear stiffness with application to random vibration of geometrically nonlinear structures, Comput. Struct. 81 (2003) 1513–1523.
[26] M.P. Mignolet, A. Przekop, S.A. Rizzi, S.M. Spottswood, A review of indirect/non-intrusive reduced order modeling of nonlinear geometric structures, J. Sound Vib. 332 (2013) 2437–2460.
[27] R.J. Kuether, Nonlinear modal substructuring of geometrically nonlinear finite, Element Models (2014).
[28] Y. Wang, X.Q. Wang, M.P. Mignolet, S. Yang, P.C. Chen, Modeling of uncertain spectra through stochastic autoregressive systems, Mech. Syst. Signal Process. 70–71 (2016) 506–526.
[29] P. Cacciola, G. Muscolino, Dynamic response of a rectangular beam with a known non-propagating crack of certain or uncertain depth, Comput. Struct. 80 (2002) 2387–2396.